Journal of Hydroscience and Hydraulic Engineering
Vol. 1, No. 1, April, 1983, pp.37-51.

THERMAL CONVECTION FOR LARGE WATER DEPTH AND LARGE RAYLEIGH NUMBERS

BY

Nobuyuki Tamai

Associate Professor, Department of Civil Engineering,
University of Tokyo, Tokyo, Japan

and

Takashi Asaeda

Research Associate, Department of Foundation Engineering,
Saitama University, Urawa, Japan

SYNOPSIS

Convection under the large Rayleigh number is studied through experiments and theoretical analysis. Flow visualization shows that buoyancy flux is transported to the convective motion by the form of vortex rings in an initial stage and then by sheet-like plumes in an equilibrium stage which is further classified into steady cell region and turbulent cell region.

The formation of initial vortex rings is explained by the extension of a linear stability theory. The representative velocity and length scales in the equilibrium state are derived in the functions of the flux-type Rayleigh number. It is also shown that the ratio of the average horizontal scale of cells to the water depth is explained by the Reynolds number defined by the maximum convective velocity in the cell.

INTRODUCTION

In lakes and reservoirs, the temperature of the water becomes uniform in winter. Diurnal stratification and nocturnal destratification near the water surface are occasionally observed in summer. This is mainly attributed to the layer-scale convection formed by the heat loss due to conduction, radiation and evaporation to the air. Since Bénard first observed renowned hexagonal cells induced by the heating, many papers have been presented and characteristics of convection with the small Rayleigh number are considerably clarified. However, convection under the large Rayleigh number has not been completely clarified because of the increase of complexity in the flow structure.

Let us review several previous results obtained under the condition of the large Rayleigh number. For the case of experiments heated from below the formation of the heat-diffusion layer in the vicinity of the bottom has been known. The mean temperature structure near a fixed boundary was predicted by Howard (8) based on the boundary-layer instability and the theory showed sufficient agreement with the measurement of Townsend and Elder. Then Sparrow et al. (16) showed that the temperature of the diffusion layer varies periodically due to the occurrence of the thermal. The occurrence of thermals was extensively examined by Spangenberg and Rowland (14), Katsaros (9), and Katsaros et al. (10) by the experiment with the cooling of an upper boundary. According to their results, sheet-like flow occurs from the cooled boundary layer just below the surface.

The mean temperature profile within the bulk of the medium and the horizontal length scale were obtained by Deardorff and Willis (4) and Fitzjarrald (6). However, the relation between sheet-like flow from the boundary and the cell struc-

tures have not been clarified yet. The purposes of this study are to determine the condition of the onset of the thermal convection in a large water body and to clarify the mechanism of the convective motion including fluctuation under the large Rayleigh number.

A part of this paper was originally published in the reference (1).

EXPERIMENTAL PROCEDURE

The experiments were performed in three types of tanks which had different scales and function. Experiments in which the maximum vertical scale of cells was smaller than about 5cm were performed in a tank of 25cm by 25cm in horizontal dimensions and 50cm high and its bottom plate was made of a 1.0mm-thick aluminum plate. As for the large scale convection whose vertical scale was 45cm at most, a tank of 90cm by 90cm in horizontal scales and 70cm high, with a 3.0mm-thick aluminum bottom plate, was utilized. On the lower side of the bottom plate, a plate rubber heater was mounted. Plates of polystyrene foam were mounted on both sides of walls and below the plate rubber heater to prevent heat exchange through the tank wall. Thickness of polystyrene plates is 3cm for the side walls and 6cm for the bottom. On the surface of the water a 3cm-thick plate was provided except the time when we took photographs from above.

Heat exchange due to conduction and radiation from the side walls of experimental tanks was estimated to be less than 1% of the heat supplied from the bottom plate, because the temperature of the water was kept within $1\sim3°C$ below that of the atmosphere.

Temperature variation on the bottom plate could not be detected by a thermistor probe the sensitivity of which was 0.05°C. The heat flux from the bottom plate was calibrated by measuring the increase of the water temperature. There was no significant difference between measurements with and without stirring.

Water temperature was measured by a thermistor linearizer circuit (Takara Thermistor Instruments Co. Ltd. E311-312-321). The probe was constructed by a circular rod of 1.0mm diameter and the time constant was less than 0.7 sec.

In most experiments the water was heated inpulsively at a constant flux. But in order to investigate the effect of the way of heating, the heat flux was gradually increased at a rate of 2.62×10^{-6} cal/(cm^2sec^2) in some runs of experiments.

The horizontal scale of the convection cell at the initial stage of the formation was observed with three ways of flow visualization. The first is the utilization of a thin film of dye solution injected on the bottom plate of an experimental tank. When a thermal begins to rise, the elongated dye film shows a periphery of a rising thermal. Several thermals tend to converge to an organized cell before long. In this converging zone the color of dye becomes dark and we can detect the outer edge of cells. The second is the phenolphthalane-method which is the modification of the one described by Baker (2). The third is the use of aluminum powder distributed in the water body. Particles of aluminum powder shine in a horizontal slit-beam of light. But if the vertical flow is strong, aluminum powder does not shine by this method. Therefore, at the ceiling level of convection cells dark lines on the picture are regarded as the converging and sinking lines of particles. No appreciable difference was found among the data obtained by these three techniques.

The vertical flow pattern and the vertical velocity of the convection were obtained by the flow visualization employing streak photography. The movement of aluminum powder was observed by utilizing an array of a vertical slit-beam of light. The falling velocity of the aluminum powder was negligibly small during the exposure time of one second at most.

FORMATION PROCESS OF CONVECTION CELLS

When the constant heat flux is added impulsively to the bottom plate, heat begins to uniformly diffuse upwards. Consequently, a thin sheet is formed on the bottom plate. The thickness of the sheet, however, does not grow indefinitely. After some quantity of heat is accumulated in a thin layer, uniformity of the layer breaks due to instability and some pairs of convection occur in the layer.

Then some plumes appear from the upward flow of convections with vortex rings on the top of them. So at the inception many vortex rings appear simultaneously. Behind each vortex ring, heated water flows into it from the bottom and deforms it into a mushroom-like shape (see Fig.1)

In a horizontal plane the position of rising vorticies constitutes vertexes of polygons. A rising vortex is associated with a strong sheet-like upward plume. In a plan view from the top of a tank, many dark polygonal patterns are observed accompanying a rising vortex ring at each vertex (see Fig.2).

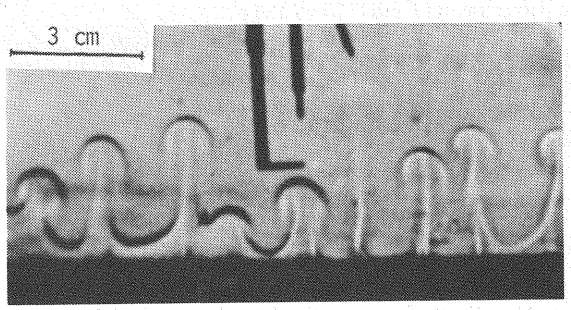

Fig.1 Vortex rings at the onset of convection

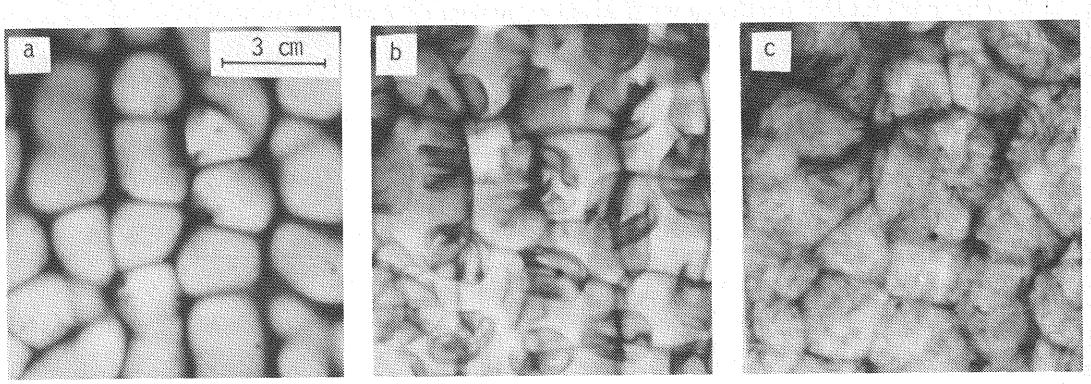

Fig.2 The horizontal view of the bottom plate at the onset of convection (a) Polygonal patterns appear at the beginning. (b) Vortex rings begin to rise at vertexes of the polygonal patterns. (c) Soon after the rising water reaches the surface, convections become in an equilibrium state.

Among these vortex rings, weak ones disappear or are absorbed into stronger ones during the rising. Associated with this process, the convective pattern on the bottom changes gradually, that is, the scale of a polygon under a strong vortex ring becomes larger, and vice versa. Between the two rising columns of water, downward flow exists to satisfy the conservation of mass. Consequently, these two neighboring flows compose a cell structure.

Soon after the front of the rising vortex reaches the water surface, the cell system enters into equilibrium condition.

INITIAL FEATURE OF VORTEX RINGS

During the initial, short period after the onset of heating, heat is transported uniformly to the water mass just above the bottom plate by not convection but diffusion and radiation. When the Rayleigh number of this layer reaches some critical value, this layer is considered to become unstable and the convection forms in the layer. The development of instability in the layer formed just above the bottom plate to which constant heat is supplied is analyzed by a linear theory with the following non-dimensional variables.

$$x = x^* h \qquad t = t^*(h^2/\kappa); \qquad u = u^*\kappa/h; \qquad T = T^*Fh/(\rho c\kappa)$$

where h is the vertical characteristic length scale; x a position vector; u a velocity vector; ρ the density; c the specific heat of water; ν the kinematic viscosity of water; κ the coefficient of thermometric conductivity of water; T the temperature; F the heat flux from the bottom plate; and a superscript * means

a nondimensional variable.

Then the dimensionless form of governing equations for the system is given as follows.

$$(\frac{1}{P_r}\frac{\partial}{\partial t} - \Delta)\Delta w = - R_{af}\Delta_1 T \tag{1}$$

$$N_u(\frac{\partial}{\partial t} - \Delta)T = - w \tag{2}$$

where P_r is the Prandtl number; R_{af} the flux-type Rayleigh number ($=\alpha Fgh^4/\rho c\kappa^2\nu$); N_u the Nusselt number ($=Fh/\rho c\kappa T_d$); T_d the temperature difference between two boundaries; α the coefficient of volume expansion due to unit temperature change; w the vertical velocity; $\Delta=\partial^2/\partial x^2+\partial^2/\partial y^2+\partial^2/\partial z^2$; $\Delta_1=\partial^2/\partial x^2+\partial^2/\partial y^2$; x and y the horizontal coordinates; z the vertical coordinate; and the superscript is omitted for the simplicity.

As the convection occurs very rapidly, boundary conditions are

$$w = 0; \quad \frac{\partial w}{\partial z} = 0 \qquad \text{at} \quad z = 0 \tag{3}$$

$$w = 0; \quad \frac{\partial^2 w}{\partial z^2} = 0 \qquad \text{at} \quad z = 1 \tag{4}$$

There are several analyses for the critical Rayleigh number R_{ac}, for example, Reid and Harris (13), Foster (7) and Sparrow et al. (15). If we follow the result of Reid and Harris, $R_{ac}=1100.7$ and the representative horizontal scale of a cell L, is given by $L=3.31h$ for the rectangular cell and $L=1.56h$ for the hexagonal cell. Therefore, L is rewritten by the following equation through the definition of the flux-type Rayleigh number. In this expression h explains the thickness of a conduction layer on the bottom.

$$L = K_1(R_{ac}\frac{\rho c\nu\kappa^2}{\alpha gF})^{1/4} \tag{5}$$

where $K_1=3.31$ for the rectangular cell and 1.56 for the hexagonal cell. Figure 3 shows the average horizontal distance of the generated vortex rings. The results obtained by the Schlieren method are concerned with two-dimensional experiments, and so the results are a little different from other results.

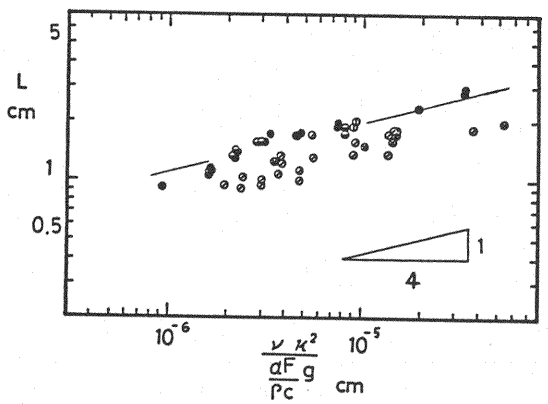

Fig.3 Average distance between vortex rings (Different symbols represent results obtained by different methods as follows: ⊘ Schlieren method, ⊗ aluminum powder by the vertical slit beam, ⊕ aluminum powder by the horizontal slit beam, ● dye method, ◒ phenolphthalane method.)

According to our experimental results, the following relationship is obtained.

$$L = 4 \sim 6(R_{ac}\frac{\rho c\nu\kappa^2}{\alpha gF})^{1/4} \tag{6}$$

The proportinal constant in Eq.6 is a little larger than predicted value as shown in Eq.5. This tendency is attributable to the following reason. If the vortex ring appears as soon as Rayleigh number reaches the critical value, the proportional constant should be nearly the same value described by Eq.5. To develop the vortex ring, however, more heat flux is needed after the threshold of instability is reached. So the Rayleigh number corresponding to the appearance of the vortex

ring is larger than that obtained in the linear stability theory. Moreover, the vortex ring does not always appear at each vertex of polygons, so the measured value of L is larger than the predicted value.

Before the stability breaks down, heat is transferred into the water body by only conduction. So the time scale T_v which elapsed before the appearance of vortex rings may be estimated from the representative length scale in the Rayleigh number. Assuming the proportionality between h and L, which is the result of the linear stability theory, T_v is obtained by Eq.6 as follows. The experimental data agreed with Eq.7.

$$T_v = 1.0 \left(R_{ac}\frac{\rho c \nu}{\alpha g F}\right)^{1/2} \tag{7}$$

CONVECTION IN AN EQUILIBRIUM STATE

Many experiments of the steady convection have been made in the region where the Rayleigh number is smaller than $100R_{ac}$. Hereafter, the water depth d is utilized for the representative length scale in the definition of the Rayleigh number. In this range of the Rayleigh number the steady cell is observed. In this experiment it is hard to measure the temperature difference between the upper and the lower side of the convective layer, so almost all results are expressed in terms of the flux-type Rayleigh number R_{af}, which is related to the usual Rayleigh number R_a as seen in $R_{af}=N_u R_a$. Here R_a is defined by $R_a=\alpha g T_d d^3/(\kappa\nu)$. As the Nusselt number is 3 to 20 in this series of experiments, $R_{af}=(3\sim20)R_a$. With the use of this relation the range of this series of experiments is $R_a=5\times10^3\sim2\times10^9$, which covers the range between the two dimensional cell region and the turbulent flow region defined by Krishnamurti (11, 12).

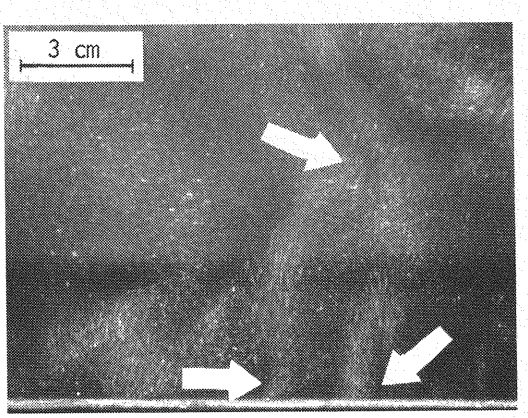

Fig.4 Sheet-like plumes in the vicinity of the bottom plate (Two plumes occurring near the bottom join each other at the mid-depth.)

According to the visualization it is observed that the flow pattern can be divided into two main classes and a threshold will be given by $R_{af}=2\times10^6$.

First, when $R_{af}<2\times10^6$, the convective pattern is in the steady state as a whole. This region is further classified into three stages as follows. When R_{af} is very small, no cell forms. Regular polygonal cells appear even if there is no cell at the beginning, as R_{af} increases. Then as R_{af} increases further, regular polygonal cells develop into meandering two dimensional cells soon after regular polygonal cells are formed. The change of the cell pattern occurs simultaneously in a horizontal plane. And these cells do not change their positions even if the coupling and enlargement of cells occur among several polygonal cells.

Next, when $R_{af}>2\times10^6$, various shapes of polygons which are composed of rising flow lines are seen. Being different from cells observed in the range of small R_{af} the shape experiences fluctuation.

The characteristics of the motion in a vertical plane can be described as follows. In case of large R_{af} the movement of each water particle shows fluctuation though the macroscopic or average feature of convection changes only very slowly. Upward convective motion is composed of many sheet-like rising plumes. Because of the rising heated water, there is a tendency that successive plumes are generated at about the same position and because of the horizontal flow near the bottom, new plumes are combined with the old one on the way of rising when they appear in the vicinity of the existing plume (see Fig.4). In this case the polygon surrounded by these plumes disappears (see Fig.5). But a new plume sometimes

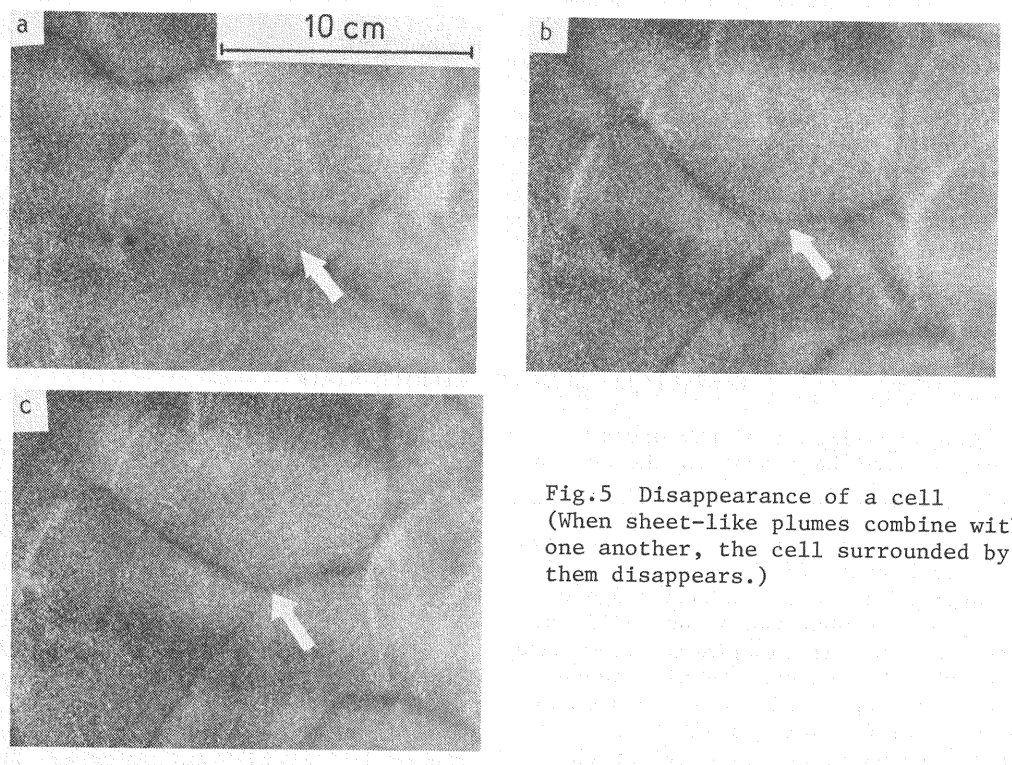

Fig.5 Disappearance of a cell (When sheet-like plumes combine with one another, the cell surrounded by them disappears.)

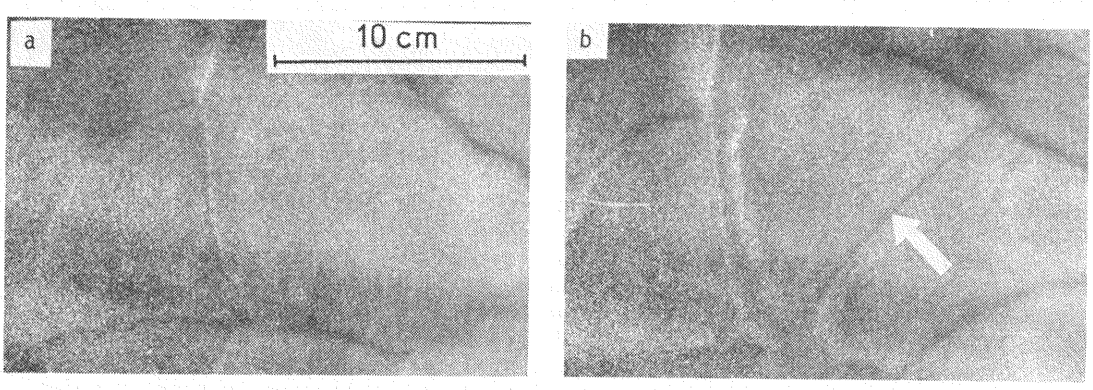

Fig.6 Appearance of a new rising flow line (A new sheet-like plume appears and divides the existing cell.)

appears at a place where there has been no plume in the vicinity. In this case one polygon is divided into two by a new sheet-like plume(see Fig.6). These two cases are main processes of the fluctuating change in the polygonal pattern.

When a new plume appears, a vortex ring forms on the top of rising water like a mushroom, so that it sometimes ceases to rise and changes its direction and then joins with another plume because the resistance against rise of vortex ring is extremely large. But when sheet-like plumes are generated frequently, no vortex ring appears on the top of it except the first one, so plumes reach the water surface and they look like a column of rising water. Figure 7 shows the three plan views of typical cell patterns taken at the same time. Figure 7(a) explains the picture taken in the illuminated horizontal plane just below the surface. Dark lines correspond to converging lines of water and along these lines downward sinking motion prevails to compensate the motion of water due to rising plumes. Figure 7(c) is the horizontal plane in the vicinity of the bottom plate, which shows

projected curves where upward flow exists as dark line. It is seen that polygons of dark lines in Fig.7(a) are intersected by polygons in Fig. 7(c) when they are superimposed, but the number of vertexes in polygons composed of converging lines is less than that observed in polygons constituted of rising sheet-like plumes. Therefore, it is considered that on the way of rising some sheet-like plumes join one another and concentrate to stronger plumes. Because of the eddies assciated with irregularity of the upward flow, Fig. 7(b) taken at the mid depth does not show clear side lines between neighboring polygons.

This set of figures shows that many plumes from rising flow lines are continuous between the bottom and the water surface, and the polygonal pattern of sheet-like plumes is closely related to the convection cells.

Hereafter, we call the region where R_{af} is larger than 2×10^6 a turbulent cell region.

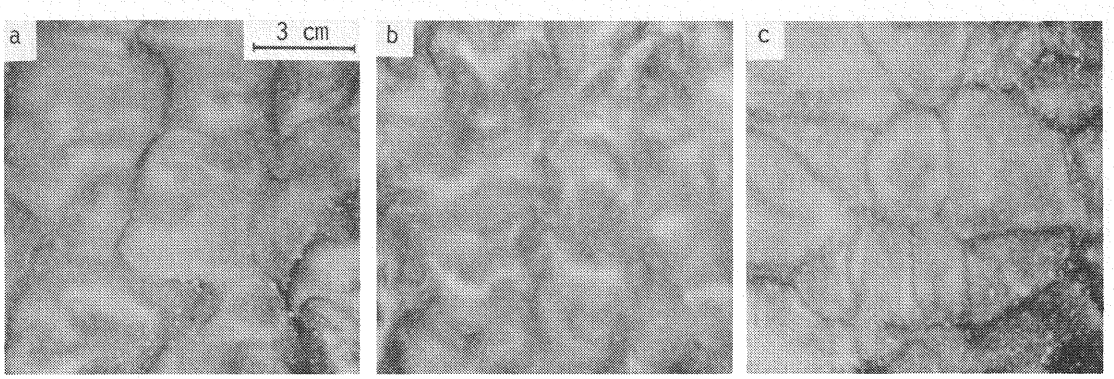

Fig.7 Three plan views of typical cell patterns taken at the same time

CHARACTERISTIC VELOCITY SCALE

As described above, the flow pattern of convection is different between the steady cell region and turbulent cell region. The magnitude of the velocity is also different in these two regions.

(i) Turbulent cell region

Figure 8 shows the relationship of the maximum convective velocity versus the buoyancy flux from the bottom plate. The maximum velocity is measured as follows. In the first step the maximum velocity shown on a particular streak-photograph is recorded. Then the average of about ten recorded values is defined as the maximum convective velocity. In this figure it is found that the maximum velocity obtained in the turbulent cell region is proportional to the 1/3-power of the added potential energy. The following relationship is obtained empirically.

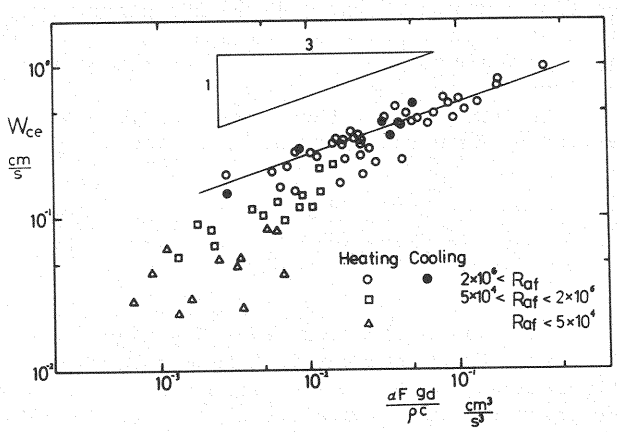

Fig.8 The maximum convective velocity versus the buoyant flux from the bottom plate (When $R_{af}>2\times10^6$, the maximum velocity of convection follows the line $W_{ce}=1.5(\frac{\alpha F}{\rho c}gd)^{1/3}$. However, for $R_{af}<2\times10^6$, the velocity is smaller than the relation.)

$$W_{ce} = 1.3(\frac{\alpha F}{\rho c}gd)^{1/3} \qquad \text{for } R_{af}>2\times10^6 \tag{8}$$

The magnitude of exponent in Eq.8 is confirmed by the following consideration. Since the moving velocity of a fluid particle reaches the maximum value around the mid depth of the layer and remains constant, the buoyancy force should be in equilibrium with the shear force experienced by a fluid particle. Buoyancy force is supplied by the heated bottom plate when the fluid moves horizontally in contact with the bottom. This relationship is expressed in Eq.9.

$$\frac{\alpha F l}{\rho c \tilde{u}} g = \text{const.}\varepsilon \frac{d\tilde{w}}{dx} \tag{9}$$

where l is the horizontal scale of the cell; $\tilde{u}$ the characteristic horizontal velocity on the bottom plate; $\tilde{w}$ the characteristic vertical velocity in the mid part of the depth; and ε the eddy viscosity coefficient. As for the averaged convection flow, the components of velocity are related to the vertical velocity by

$$\tilde{u} = \frac{\partial^2\tilde{w}}{a^2\partial x\partial z}\ ; \qquad \tilde{v} = \frac{\partial^2\tilde{w}}{a^2\partial y\partial z} \tag{10}$$

where a is the absolute value of horizontal wave number, that is , $a^2=a_x^2+a_y^2$, where a_x and a_y are two horizontal components. So,the relation $\tilde{u}=(l/d)\tilde{w}$ approximately holds. If we assume $\varepsilon=\text{const.}\tilde{w}l$, Eq.9 yields the following relation.

$$\frac{\alpha F}{\rho c}gd = \text{const.}W_{ce}^3 \tag{11}$$

In other words, this relation means that the buoyancy flux added to the bottom plate is transferred to the kinetic energy of the movement of the water particles in the convection layer at constant rate in the turbulent cell region.

(ii) Steady cell region

The maximum convection velocity in the steady cell region is not expressed as a function of buoyancy flux from the bottom plate only, as shown in Fig.8. Since the flow pattern of the cell in the steady cell region looks like that of the marginal state cell whose Rayleigh number is a little larger than the critical Rayleigh number, the hydraulic features of the cell are compared with the previous results.

The amplitude of the convection velocity in the marginal state is theoretically derived by Chandrasekhar (3) as follows.

$$W_{ce}^2 = \frac{\kappa^2 a}{d^2}\frac{\int_0^1\tilde{W}\Delta^2\tilde{W}dz}{\int_0^1\tilde{W}^2(\Delta^2\tilde{W})^2dz\cdot\{\int_0^1\tilde{W}\Delta\tilde{W}dz\}^2}(\frac{R_{af}}{N_u} - R_{afc}) \tag{12}$$

where R_{afc} is the critical flux Rayleigh number and W_{ce} is the normalized vertical velocity. Since the vertical flow pattern is composed of concentric circles in this region, the normalized vertical velocity is assumed in the following form referring to experimental results.

$$\tilde{W} = \sin a\pi z \tag{13}$$

Substituting Eq.13 to Eq.12, the amplitude of the vertical velocity is obtained as follows.

$$W_{ce} = 2\frac{\kappa a}{d}\frac{1}{\pi^2+a^2}\{\frac{R_{af}}{N_u} - \frac{(\pi^2+a^2)}{a^2}\}^{1/2} \tag{14}$$

Figure 9 shows the comparison of experimental results with calculated results. As for the Nusselt number, N_u, the experimental results of Silveston (Chandrasekhar

(3)) is utilized. The predicted result by Eq.14 is approximately in agreement with experimental results except for the data in the turbulent cell region. However, Eq.14 still contains the internal parameter, a, which is proportional to the ratio of the horizontal scale to the vertical one. On this quantity, we will discuss later in the next section

LENGTH SCALE OF THE CONVECTION

(i) Turbulent cell region

Deardorff and Willis (4) and Fitzjarrald (6) defined the horizontal scale as the largest peak of the co-spectrum calculated from the record of horizontal distribution of temperature and vertical velocity. However, since the generation of plumes is not a continuous stochastic process but it shows quite intermittent nature, the length scale from the largest peak of the co-spectrum is considered to be several times larger than the averaged value of the horizontal distance between sheet-like plumes, which corresponds to representative length scale of convection cells. Here, we examine the characteristic length scale of the distance between sheet-like plumes.

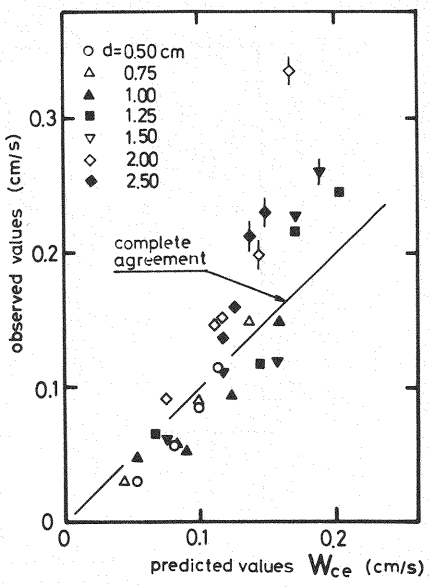

Fig.9 The comparison of the observed convective velocity with prediction by Eq.14 (¦ means the results for $R_{af}>2\times10^6$, which is off the caluculated results.)

The average value of the length of sides of the polygons formed by sheet-like plumes is defined as the horizontal scale of the cell, l. The typical frequency distribution of the length of sides of polygons during a second is shown in Fig.10 where l' is an individual length of sides of polygons. Judging from the figure, the distribution function is approximately expressed as the normal distribution around the mean value, and so the average value of a series of records is adopted to calculate the value of l.

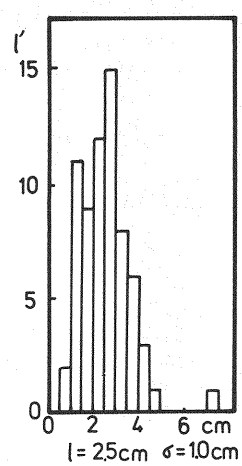

Fig.10 The distribution of length of sides of polygons (The average value of the horizontal scale l is 2.5cm and the standard deviation is 1.0cm.)

Figure 11 shows the ratio of the horizontal scale to the vertical scale as a function of the product of the square root of the flux Rayleigh number and the inverse of the Prandtl number. As for the vertical length scale the whole depth of the layer is taken when the temperature of the layer is homogeneous, and the average thickness of the moving layer is taken when there is a thermocline in the layer.

In Fig.11 it is seen that l/d decreases with R_{af} and is expressed by a function stated below, for the turbulent cell region.

$$\frac{l}{d} = 7.1(R_{af}^{1/2} P_r^{-1})^{-1/3} = 7.1\left(\frac{\alpha F\, gd^4}{\rho c\, \nu^3}\right)^{-1/6} \qquad (15)$$

In order to verify the suitability of the definition of the horizontal length scale, we checked the appliability of Eq.15 using $S^{1/2}$ instead of l, where S is area of each polygon. The obtained diagram showed the same relationship as Fig.11.

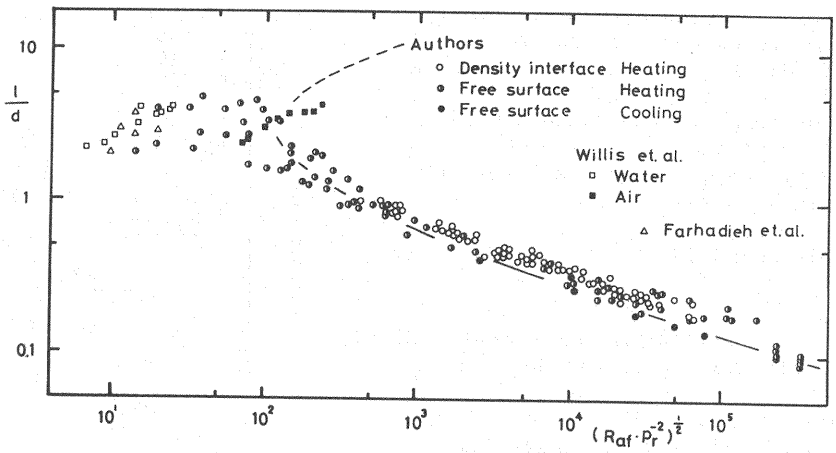

Fig.11 The ratio of the horizontal scale to the vertical scale of the convection as a function of $R_{af}^{1/2} P_r^{-1}$ (●◑○ represent the results of rapid constant heating, and others represent the results of the gradual heating. Δ shows the experimental result by Farhadieh and Tankin (5), □ the results by Willis et al.(17) and ■ the results of experiments utilizing air by Willis et al. R_a used in previous papers is converted to R_{af}.)

The theoretical basis of Eq.15 is explained as follows. For the sake of simplicity let us consider only one representative cell. Since the convective motion is strong in the turbulent state, almost all heat supplied from the bottom is transferred by the advective type of motion. Therefore, the temperature in the convective layer is supposed to be uniform and the contribution of conduction of heat is negligible. So the energy released by the buoyancy force due to the bottom heating in a unit time is expressed as

$$P = -\frac{\alpha F}{2\rho c} Sdg \tag{16}$$

The rate of viscous dissipation in the convection layer is defined by

$$\Phi = -\nu\int_0^d (\langle u\nabla u\rangle + \langle v\nabla v\rangle + \langle w\nabla w\rangle)dz\cdot S \tag{17}$$

where angular brackets signify that the enclosed quantity is averaged over the horizontal plane and $\nabla=\partial/\partial x+\partial/\partial y+\partial/\partial z$. Considering the average convection flow, we use the cellular flow pattern proposed by Chanrasekhar for simplicity. The horizontal components of velocity are related to the vertical one as follows.

$$u = \frac{1}{a^2}\frac{\partial^2 w}{\partial x\partial z}\ ; \qquad v = \frac{1}{a^2}\frac{\partial^2 w}{\partial y\partial z} \tag{18}$$

To be specific, let w be

$$w = W(z)\ f(x, y) \tag{19}$$

where f is a distribution function in a horizontal plane and satisfies $\Delta_1 f=-a^2 f$. As an example, let us take a prismatic cell. Horizontal boundary conditons are

$$w = W(z) \quad \text{at the points, } (\pm n\ell,0),\ \{\pm(n+\tfrac{1}{2})\ell,\ \tfrac{1}{2}\pm\ell\},\ \text{etc.} \tag{20-a}$$

$w = -W(z)$ at the points, $\{\pm(n+\frac{1}{2})\ell, 0\}$, $(\pm n\ell, \pm\frac{1}{2}\ell)$, etc. (20-b)

$w = 0$ along the lines, $x=\pm\frac{1}{4}\ell$, $\pm\frac{3}{4}\ell$, etc. and

$y=\pm\frac{1}{4}\ell$, $\pm\frac{3}{4}\ell$, etc. (20-c)

where n is an integer. So the three components of the velocity are given by

$$\begin{cases} u = -\frac{\ell}{4\pi}\frac{d}{dz}W(z)\sin\frac{2\pi}{\ell}x\cos\frac{2\pi}{\ell}y \\ v = -\frac{\ell}{4\pi}\frac{d}{dz}W(z)\cos\frac{2\pi}{\ell}x\sin\frac{2\pi}{\ell}y \\ w = W(z)\cos\frac{2\pi}{\ell}x\cos\frac{2\pi}{\ell}y \end{cases} \quad (21)$$

Substituting Eq.21 into Eq.17, we obtain

$$\Phi = S\frac{\nu}{4a^2\pi^2}\int_0^d\{(\frac{d^2}{dz^2} - a^2)W(z)\}^2dz \quad (22)$$

According to Eq.8, W(z) is expressed as

$$W(z) = 1.3(\frac{\alpha F}{\rho c}gd)^{1/3}\sin\frac{\pi}{d}z \quad (23)$$

Since the convection is in an equilibrium state, the energy released by the buoyancy force is necessary to be balanced by the energy dissipation.

$$P = \Phi \quad (24)$$

Substitution of Eqs.16, 22 and 23 into Eq.24 makes the following relation.

$$\frac{\alpha F}{2\rho c}Sgd = \frac{1.3^2}{64}\pi^2 S\ell^2\nu(\frac{\alpha F}{\rho c}gd)^{2/3}\cdot(\frac{1}{d^2} + \frac{8}{\ell^2})^2 d \quad (25)$$

The roots of this equation are given by

$$\frac{\ell}{d} = 2\sqrt{2}\left[\{\frac{2}{(1.3\pi)^2}R^{1/3} - 1\} \pm 2\{\frac{1}{(1.3\pi)^4}R^{2/3} - \frac{1}{(1.3\pi)^2}R^{1/3}\}^{1/2}\right]^{1/2} \quad (26)$$

where $R=R_{af}/P_r{}^2$. The condition which makes Eq.26 real is

$$R_{af} \geq (1.3\pi)^6 P_r{}^2 = 2.08 \times 10^5 \quad (27)$$

The value of the right-hand side of Eq.27 is considered to be the minimum flux-Rayleigh number under which the turbulent convection cell exists. Making use of this value described by R_{aft}, we can rewrite Eq.26 in the form

$$\frac{\ell}{d} = 2\sqrt{2}\{2A - 1 \pm 2(A^{2/3} - A^{1/3})^{1/2}\}^{1/2} \quad (28)$$

... for the rectangular convection cell

Similarly for the two dimensional roll cell, we obtain

$$\frac{l}{d} = 2\{2A - 1 \pm 2(A^{2/3} - A^{1/3})^{1/2}\}^{1/2} \qquad (29)$$

··· for the two dimensional convection cell

where $R_{aft}=8(1.3\pi)^6 P_r{}^2$ and $A=R_{af}/R_{aft}$. The curve which represents Eq.28 is shown in Fig.11 by a solid line(a lower branch) and a dashed line(an upper branch). In these two branches it is considered that the actual convection cell follows the branch energy level of which is lower than another, since it changes its shape easily in the turbulent cell region. As the potential energy is the same value in these two branches, we consider the kinetic energy, considering Eqs.21, 23, and 28. Then, we obtain

$$E_k = \frac{\rho}{32} W_{ce}{}^2\{2A^{1/3} + 2(A^{2/3} - A^{1/3})^{1/2} + 1\} \qquad (30)$$

··· for the upper branch

$$E_k = \frac{\rho}{32} W_{ce}{}^2\{2A^{1/3} - 2(A^{2/3} - A^{1/3})^{1/2} + 1\} \qquad (31)$$

··· for the lower branch

Judging from Eqs.30 and 31, the lower one is more stable, so it fits more suitably to experimental results.

As described above, the length scale ratio can be expressed as a function of external parameters. However, taking account of Eq.8, it can be rewritten as a function of the cell Reynolds number, as follows.

$$\frac{l}{d} = 2\sqrt{2}\{2B^3 - 1 - 2(B^2 - B)^{1/2}\}^{1/2} \qquad (32)$$

where $R_e=W_{ce}d/\nu$ and $B=R_e/(1.3^3\pi^2)$. Therefore, it can be said that the shape of convection cell is dependent on the cell Reynolds number in this region. As for the representative velocity scale in the Reynolds number, an experimentally derived expression of Eq.8 is utilized. A further study, however, is still needed for the detailed discussion on the applicability of Eq.8 to a large-scale field problem.

(ii) Steady cell region

Different from turbulent cell region, Fig.11 shows that the length scale ratio l/d is not a simple function of R_{af} and P_r in the steady cell region. However, it is supposed that l/d is strongly correlated to the Reynolds number $R_e=W_{ce}d/\nu$ just like in turbulent cell region.

Figure 12 shows the relation between l/d and R_e with the use of the experimental result in W_{ce}. The following relationship is obtained by this experiment.

$$\frac{l}{d} = 2.0\left(\frac{W_{ce}d}{\nu}\right)^{1/3} = 2.0\, R_e{}^{1/3} \qquad (33)$$

Utilizing Eqs.14 and 33, we have

$$\left(\frac{l}{d}\right)^8\{\left(\frac{l}{d}\right)^2 + 8\}^2 = \frac{2^{11}}{(\pi P_r)^2}\left[\frac{R_{af}}{N_u}\left(\frac{l}{d}\right)^4 - \frac{\pi^4}{8}\{\left(\frac{l}{d}\right)^2 + 8\}^3\right] \qquad (34)$$

In the case of $R_{af}/N_u \gg l/d$, the length scale ratio l/d and the cell Reynolds number, that is, nondimensionalized velocity are rewritten by external parameters as follows.

$$\frac{l}{d} = \sqrt{2}\{(1 + \frac{8\sqrt{2}}{\pi} N)^{1/2} - 1\}^{1/2} \qquad (35)$$

$$\frac{W_{ce}d}{\nu} = \frac{\sqrt{2}}{4}\{(1 + \frac{8\sqrt{2}}{\pi} N)^{1/2} - 1\}^{3/2} \qquad (36)$$

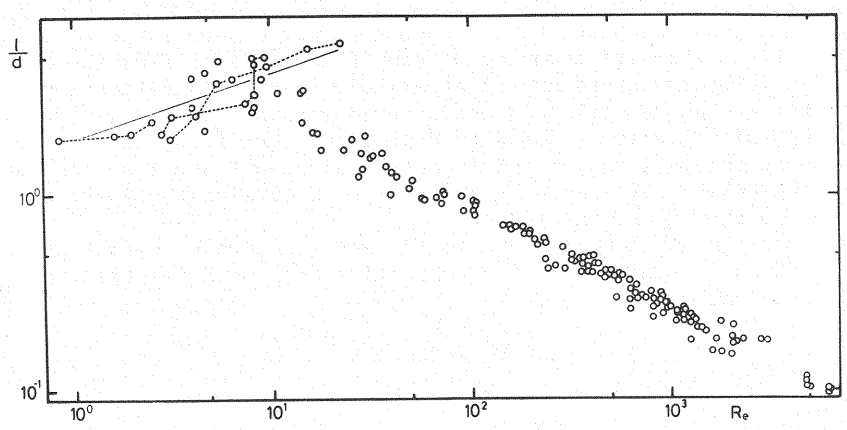

Fig.12 The scale ratio rearranged by the Reynolds number (A solid line shows Eq.33, and a dashed line shows the process of variation when heat flux is gradually increased.)

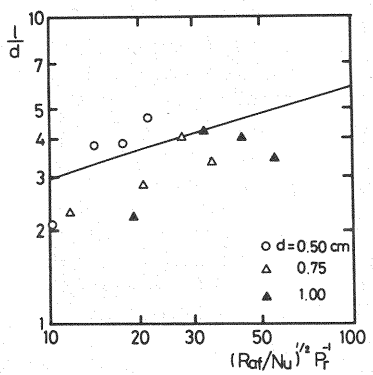

Fig.13 The scale ratio expressed as a function of the external parameters in the range of $R_{af}<2\times10^6$ (A solid line shows Eq.35.)

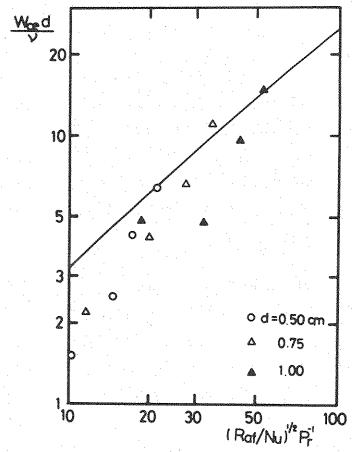

Fig.14 The nondimensional velocity expressed as a function of the external parameters in the range of $R_{af}<2\times10^6$ (A solid line shows Eq.36.)

where $N=(R_{af}/N_u)^{1/2}/P_r$.

Figures 13 and 14 show the comparison of Eqs.35 and 36 with the experimental results. They show that Eqs. 35 and 36 are fairly good prediction for the ratio of length scale and the maximum convective velocity in the steady cell region.

It is concluded that l/d is expressed by not a simple function of R_{af} but a function of R_e in both the turbulent cell region and the steady cell region, though the functional form differs in each region.

CONCLUSIONS

1) At the onset of convection, many vortex rings appear and their separations from the bottom plate occur almost simultaneously. The functional forms for the spacial interval of vortex rings and the time scale of the vortex formation are deduced from the linear stability theory. Numerical coefficients are determined by the measured data.

2) In an equilibrium state, the characteristics of convection change when R_{af} exceeds the value of 2×10^4. In the region that R_{af} is less than 2×10^4 the cell pattern is regular and streamlines in a vertical plane are coaxial. When R_{af} is

larger than 2×10^6, on the other hand, convective motion shows the nature of turbulence. Convective cells are composed of many plumes rising from the bottom and hydraulic quantities concerned are fluctuating. Even in this turbulent cell region it is seen that the depth scale convection exists as a whole.

3) The characteristic velocity of the convection is derived from marginal state theory in the steady cell region and from the balance of shear stress and buoyant force in the turbulent cell region. In order to determine the coefficients, we need to refer to the experimental results.

4) The ratio of the horizontal scale to the vertical scale is found to be a function of R_e defined by the motion of a convective cell both in steady cell region and in the turbulent cell region.

ACKNOWLEDGMENTS

It is a pleasure to record our thanks to Associate Professor S. Ikeda at Saitama University for his comments, and to Messrs. Y. Takahashi and F. Abe for their help in performing experiments.

The work was partly supported by a Research Grant of the Ministry of Education, Science and Culture.

REFERENCES

1. Asaeda, T., N. Tamai, and Y. Takahashi : On the thermal convection of an equilibrium state for large water depth and large Rayleigh number, Proc. Japan Soc. Civil Eng., Vol.323, pp.121-131, 1982 (in Japanese).
2. Baker, D.J. : A technique for the precise measurement of small fluid velocities, J. Fluid Mech., Vol.26, pp.573-575, 1966.
3. Chandrasekhar, S.: Hydrodynamic and Hydromagnetic Stability, Oxford Univ. Press, 1966.
4. Deardorff, J.W., and G.E.Willis : Investigation of turbulent thermal convection between horizontal plates, J. Fluid Mech., Vol.28, pp.675-704, 1967.
5. Farhadieh, R. and R.S. Tankin : Interferometric study of two-dimensional Bénard convection cells, J. Fluid Mech., Vol.66, pp.739-752, 1974.
6. Fitzjarrald, D.E. : An experimental study of turbulent convection in air, J. Fluid Mech., Vol.66, pp.693-719, 1976.
7. Foster, T.D. : The effect of initial conditions and lateral boundaries on convection, Phys. Fluids, Voll.112, pp.2482-2487, 1969.
8. Howard, L.N. : Convection at high Rayleigh number, Proc. 11th Int. Cong. Applied Mech., Munich, pp.1109-1115, 1964.
9. Katsaros, K.B. : Turbulent free convection in fresh and salt water, J. Phys. Ocean., Vol.3, pp.613-626, 1978.
10. Katsaros, K.B., W.T. Liu, J.A. Businger, and J.E. Tillman : Heat transport and thermal structure in the interfacial boundary layer measured in an open tank of water in turbulent free convection, J. Fluid Mech. Vol.33, pp.311-335, 1977.
11. Krishnamurti, R. : On the transition to turbulent convection, Part 1-The transition from two- to three-dimensional flow, J. Fluid Mech. Vol.42, pp.295-307, 1970.
12. Krishnamurti, R. : On the transition to turbulent convection, Part 2-The transition to time-dependent flow, J. Fluid Mech. Vol.42, pp.309-320, 1970.
13. Reid, W.H. and D.L. Harris : Some further results on the Bénard problem, Phys. Fluids, Vol.1, pp.102-110, 1958.
14. Spangenberg, W.G. and W.R. Rowland : Convective circulation in water induced by evaporating cooling, Phys. Fluids, Vol.4, pp.743-750, 1961.
15. Sparrow, E.M., R.J. Goldstein, and V.K. Jonsson : Thermal instability in a horizontal fluid layer, J. Fluid Mech., Vol.18, pp.513-528, 1964.
16. Sparrow, E.M., R.B. Husar, and R.J. Goldstein : Observations and other characteristics of thermals, J. Fluid Mech., Vol.41, pp.793-800, 1970.
17. Willis, G.E., J.E. Deardorff, and R.C. Somerville : Roll diameter depencence in Rayleigh convection and its effect upon the heat flux, J. Fluid Mech., Vol.54, pp.351-357, 1972.

APPENDIX-NOTATION

The following symbols are used in this paper:

- a = the absolute value of the horizontal wave number;
- a_x, a_y = two horizontal components of a;
- A = R_{af}/R_{aft};
- B = $R_e/(1.3^3\pi^2)$;
- c = the specific heat of water;
- d = the water depth;
- E_k = the kinetic energy of a convection cell;
- F = the heat flux from the bottom plate;
- g = the acceleration of gravity;
- h = the vertical characteristic length;
- l = the horizontal scale of a cell;
- L = average distance between vortex rings on the bottom plate;
- n = an integer;
- N_u = the Nusselt number;
- N = $(R/N_u)^{1/2} = \{R_{af}/(N_u P_r^2)\}^{1/2}$;
- P = the energy released by the buoyancy;
- P_r = the Prandtl number;
- R_a = the usual Rayleigh number defined with the temperature difference between the boundaries;
- R_{ac} = the critical Rayleigh number;
- R_{af} = the flux-type Rayleigh number;
- R_{aft} = the minimum flux-type Rayleigh number in the turbulent cell region;
- R_e = the cell Reynolds number;
- R = R_{af}/P_r^2;
- T = the temperature of water;
- T_v = the time scale elapsed before the appearance of vortex rings;
- u = a velocity vector(u,v,w);
- (u,v,w) = the characteristic velocity components in a cell;
- $W(z)$ = the vertical convection velocity in a cell;
- W_{ce} = the maximum vertical velocity in a cell;
- x = a position vector(x,y,z);
- α = the coefficient of volume expansion of water due to temperature;
- ε = the eddy viscosity;
- κ = the coefficient of thermometric conductivity of water;
- ν = the kinematic viscosity of water;
- ρ = the density of water; and
- Φ = the energy dissipation due to viscosity.